Table II. Stages of Development of Dezincification of Naturally Passivated Cu_{75}-Zn_{25} in 3% NaCl

(1) Migration to subsurface and surface of Zn^{2+} from bulk alloy to form ZnO.
(2) Dissolution of some of the protective (passivating) oxides: (A) all Cu^{2+} quickly dissolved (~5 h, 3% NaCl); (B) a little of the Cu^{+} may dissolve; (C) some of (original) ZnO also dissolves
(3) Extensive thickening of ZnO sublayer.
(4) New, thicker Cu oxide layer forms below surface layer of ZnO.
(5) Overlap of layer boundaries increases dramatically.
(6) Termination of surface secretion of Zn.
(7) Island growth of clusters of ZnO at outer surface incapsulating some Cu oxides.

dezincification of α-brass under these conditions. The stages of this process are expressed in Table II. Detailed arguments for the above conclusions will appear elsewhere.[9]

An important, as of yet unanswered, question concerns the *source* of the oxygen that produces the extensive growth of oxidized Zn (and Cu) revealed during the onset of dezincification. As mentioned above, this oxygen, no doubt, also plays a major role in the diffusion of the ions (or atoms) that necessarily precedes oxide formation. Unfortunately, at present, no definite conclusion may be drawn concerning this question; however, the experimental features do permit reasonable speculations about the oxygen source. First, it is apparent that the oxygen in question must arise during one (or more) of three possible periods: it is (1) adsorbed before immersion, (2) picked up during immersion, or (3) adsorbed following immersion but before insertion into the spectrometer. The first source is probably not important since there is too little unreacted oxygen on the outersurface of the passivated alloy to produce the relatively thick oxide layers realized after immersion. The progressive thickening of the oxide layers formed during increased exposure to the salt solution would seem to exclude both (1) and (3) as major sources of the reactive oxygen. In addition, dramatic variations in the exposure of the coupons to oxygen during stages 1 and 3 did not seem to affect any of the dezincification growth features. It seems certain, therefore, that most (if not all) of the oxygen producing the oxides formed during the onset of dezincification comes into contact with the passivated brass during the immersion in the salt solution. This does not answer the question of the *source* of the reactive oxygen, which may come from either dissolved O_2 or the electrochemical breakdown of H_2O. It has already been demonstrated that the dezincification process in question is of electrochemical rather than chemical origin. Thus, the NaCl solute is needed in order to produce the reactions (in the time frame of the present study). Crude attempts to simulate real seawater by agitating the solution during immersion altered the rate of growth and apparent thickness but not the ordering of the layers. These observations seem to favor a reaction based upon dissolved oxygen; however, further, more carefully controlled experiments (during which the amount of dissolved O_2 is both measured and varied) are needed to unequivocally establish the source.

In addition to the uncertainty as to the source of the oxygen, it should be noted that the present study concerns only the behavior of naturally passivated α-brass during the *initial* stages of dezincification as produced under conditions that crudely simulate *static* seawater. The results and proposed mechanism may be significantly different if (1) the zero-valent [Cu(0)Zn(0)] surface is the one exposed to the salt solution; (2) other types of Cu-Zn brass (e.g., α-β, β, Admiralty, etc.) are employed in the process; (3) a controlled turbulent solution (more representative of true seawater) is employed; (4) single-crystal Cu-Zn faces or large grain-sized surfaces of the polycrystalline brass are used; (5) other metallurgical aspects such as the number of defects and the state of cold working are markedly varied; and/or (6) the pH and temperature of the solution are varied. Studies in these various areas are needed before a completely general mechanism for the onset of dezincification may be realized.

Registry No. α-Brass, 82823-80-1; ZnO, 1314-13-2.

A New Type of Trinuclear Cluster Compound: The Incomplete Bicapped (or Hemicapped) Structure in $[W_3O(O_2CCH_3)_6(H_2O)_3]ZnBr_4 \cdot 8H_2O$

Michael Ardon,*[1a] F. Albert Cotton,*[1b] Zvi Dori,*[1c] Anne Fang,[1b] Moshe Kapon,[1c] George M. Reisner,[1c] and Miriam Shaia[1c]

Contribution from the Department of Chemistry, The Hebrew University, Jerusalem, Israel, The Technion-Israel Institute of Technology, Haifa, Israel, and the Department of Chemistry, Texas A&M University, College Station, Texas 77843. *Received December 29, 1981*

Abstract: Small amounts of a new, dark blue, tritungsten cluster cation have been obtained as a byproduct in the preparation of the well-known $[W_3O_2(O_2CCH_3)_6(H_2O)_3]^{2+}$ ion. This new species has been isolated in the form of the isomorphous $[W_3O(O_2CCH_3)_6(H_2O)_3]MBr_4 \cdot 8H_2O$ compounds (M = Fe, Zn), and the structure of the zinc-containing compound has been fully determined by X-ray crystallography. The crystals belong to space group $C2/c$ with the following unit cell dimensions: a = 13.218 (4) Å, b = 16.231 (5) Å, c = 17.722 (5) Å, β = 105.34 (3)°. The calculated density, 2.711 g cm^{-3}, for the above formula (Z = 4) agrees well with that measured, 2.717 g cm^{-3}. The trinuclear cation has crystallographic 2 (C_2) symmetry, but approximates closely to C_{3v} symmetry, with the following average principal dimensions (Å): W-W, 2.710 [4]; W-O(cap), 1.96 [2]; W-O(acetate), 2.07 [1]; W-O(H_2O), 2.16 [1]. The electronic structure of the hemicapped species can be considered similar to that of the bicapped species except that in place of three bonds to a second capping atom there is an empty e orbital and a filled a_1 orbital that has a moderate bonding character with respect to the W_3 triangle.

Work in these laboratories[2-7] and elsewhere[8-11] within the past few years has shown that the elements molybdenum and tungsten,[12] in oxidation states of IV or thereabouts, have a marked predilection to form trinuclear cluster species. What is even more

(1) (a) The Hebrew University. (b) Texas A&M University. (c) The Technion-Israel Institute of Technology.

(2) Bino, A.; Cotton, F. A.; Dori, Z. *J. Am. Chem. Soc.* **1978**, *100*, 5252.
(3) Bino, A.; Cotton, F. A.; Dori, Z. *Inorg. Chim. Acta* **1979**, *33*, L133.

0002-7863/82/1504-5394$01.25/0 © 1982 American Chemical Society

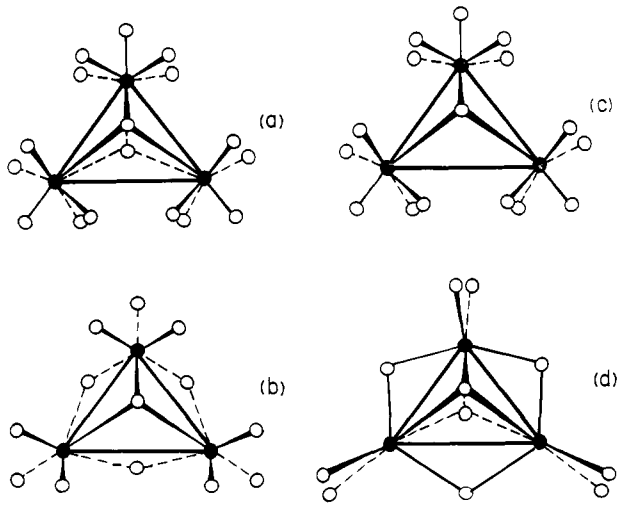

Figure 1. Prototypal representations of the four types of trinuclear cluster structures known for molybdenum and/or tungsten compounds. (a) The bicapped structure found in $[M_3X_2(O_2CR)_6(H_2O)_3]^{n-}$ species. (b) The trigonal M_3O_4 type found in, for example, the Mo (IV) aquo ion. (c) The hemicapped structure reported here for the first time. (d) The structure found in the $Mo_3O(OR)_{10}$ compounds of Chisholm.

remarkable is that these cluster species, while they are all based on an equilateral M–M bonded triangle of metal atoms, are of three different structural types with respect to the ligand arrangements. The three reported types are shown in Figure 1 as (a), (b), and (d). In this paper we report that there is still another type, shown schematically as (c) in Figure 1. This new type might be considered as a variant of (a) in which one capping group is absent. Since the a-type structure has been called the bicapped structure, this one might be called the hemibicapped, or, more simply, the hemicapped structure.

We shall describe here the method by which this new type of cluster species was obtained, present a structural characterization of the compound $[W_3O(O_2CCH_3)_6(H_2O)_3]ZnBr_4 \cdot 8H_2O$, and discuss the electronic structure of the cluster cation on the basis of a Fenske–Hall[15] molecular orbital calculation.

Experimental Section

Preparation. Tungsten hexacarbonyl (1.0 g) was refluxed under nitrogen for 24 h in 100 mL of a 1:1 mixture of acetic acid/acetic anhydride to which 2 mL of triethylamine had been added. After cooling, the reaction mixture was hydrolyzed with 200 mL of water over a period of 8–12 h, still under nitrogen. The mixture was now filtered in air and passed through a Dowex 50W-X2 cation-exchange column. The blue band that adsorbed to the column was washed with 0.5 M HCl and then eluted with 2 M HCl. For elimination of traces of $[W_3O_2(O_2CCH_3)_6(H_2O)_3]^{2+}$, this eluate was diluted with 200 mL of water and passed again through the cation-exchange column and the blue band eluted with 2 M HBr. Several grains (ca. 20 mg) of $ZnBr_2$ were added to the elutant. Slow evaporation under vacuum yielded 50–70 mg of beautiful, dark blue crystals of the title compound.

Table I. Atomic Positional Parameters[a]

atom	x	y	z
W(1)	3111 (5)	28680 (4)	32875 (4)
W(2)	0 (0)	43189 (6)	25000 (0)
Br(1)	4530 (2)	5082 (2)	6351 (1)
Zn	5000 (0)	5925 (2)	7500 (0)
Br(2)	6498 (2)	6779 (2)	7481 (2)
O(1)	827 (8)	1971 (7)	1816 (7)
O(2)	751 (10)	2212 (7)	4388 (7)
O(3)	1362 (8)	1975 (7)	3110 (7)
O(4)	1677 (9)	3427 (8)	3921 (7)
O(5)	−522 (9)	3446 (7)	3957 (7)
O(6)	1413 (9)	4633 (8)	3285 (6)
O(7)	−758 (10)	4641 (8)	3328 (7)
O(8)	0 (0)	5649 (11)	2500 (0)
O(9)	−876 (17)	3337 (14)	2532 (13)
C(1)	1967 (17)	4142 (13)	3807 (12)
C(2)	−900 (13)	4169 (12)	3873 (10)
C(3)	1418 (16)	1707 (12)	2455 (11)
C(4)	2210 (14)	1030 (12)	2430 (11)
C(5)	−1540 (19)	4498 (15)	4389 (13)
C(6)	2987 (15)	4467 (14)	4316 (12)
Ow(1)	−151 (17)	6744 (13)	1360 (13)
Ow(2)	1581 (14)	3166 (12)	5630 (10)
Ow(3)	−2673 (21)	2154 (14)	4247 (12)
Ow(4)	−697 (19)	1382 (19)	4893 (15)

[a] Fractional coordinates for the W atoms are $\times 10^5$ and for all others $\times 10^4$.

Table II. Bond Distances for Compound I (Angstroms)

W(1)-W(2)	2.715 (1)	W(2)-O(9)	1.98 (2)
W(1)-W(1)′[a]	2.701 (1)	O(1)-C(3)	1.27 (2)
W(1)-O(1)′	2.07 (1)	O(3)-C(3)	1.26 (2)
W(1)-O(2)	2.17 (1)	O(4)-C(1)	1.25 (2)
W(1)-O(3)	2.09 (1)	O(6)-C(1)	1.29 (2)
W(1)-O(4)	2.07 (1)	O(5)-C(2)	1.27 (2)
W(1)-O(5)	2.05 (1)	O(7)-C(2)	1.29 (2)
W(1)-O(9)	1.93 (2)	C(1)-C(6)	1.51 (2)
W(1)-O(9)′	1.96 (2)	C(2)-C(5)	1.50 (3)
W(2)-O(6)	2.08 (1)	C(3)-C(4)	1.53 (3)
W(2)-O(7)	2.06 (1)	Zn-Br(1)	2.400 (3)
W(2)-O(8)	2.16 (2)	Zn-Br(2)	2.424 (3)

[a] Atoms labeled with primes are related to the reference atoms by twofold symmetry.

Crystal Data and Structure Determination. The crystals were dark prisms having well-developed faces. To reduce absorption, a small fragment of irregular but quasi-spherical shape having an average diameter of 0.12 mm was cut and mounted on a Phillips PW 1100/20 four-circle diffractometer. Preliminary examination showed that the crystal system was monoclinic, and accurate cell dimensions were determined from 25 carefully centered reflections. The lattice parameters thus obtained were $a = 13.218$ (4) Å, $b = 16.231$ (5), Å, $c = 17.772$ (5) Å, $\beta = 105.34$ (3)°. The systematic absences were indicative of either of the space groups Cc or $C2/c$. Subsequent solution and refinement showed that it belongs to space group $C2/c$. With four molecules per unit cell $\rho_{calcd} = 2.711$ g cm^{-3}; ρ_{obsd} was found to be 2.717 g cm^{-3} by flotation in toluene/1,1,2,2-tetrabromoethane. The compound $[W_3O(O_2CCH_3)_6(H_2O)_3]FeBr_4 \cdot 8H_2O$, which can be prepared similarly, was found to be isomorphous. Intensity data were collected in the rage of $5° \leq 2\theta \leq 50°$ by use of graphite-monochromated Mo Kα radiation and the $\omega/2\theta$ scan mode. Three standard reflections measured every 2 h were stable. Lorentz and polarization corrections were applied to the intensity data, but no absorption corrections were made. A ψ scan at a low angle reflection showed no remarkable variations in intensity. All data processing and other calculations were carried out by using the SHELX-77[13] system of programs.

The structure was solved by the heavy-atom technique. A three-dimensional Patterson map yielded the positions of the W atoms. All the remaining nonhydrogen atoms were located from successive difference Fourier maps. Anisotropic refinement of all the non-hydrogen atoms except the capping oxygen, O(9), which was kept isotropic, converged to a final R factor of 0.066 ($R_w = 0.056$). The final statistical weights were $w = 1.296/[\sigma^2(F_o) + 0.00062F_o^2]$. A 3σ cutoff was used throughout the refinement. The number of unique reflections used in the last cycle of least squares was 2451, and the number of variables was 201. No unusually high correlations were noted between any variables in the final

(4) Bino, A.; Cotton, F. A.; Dori, Z. *J. Am. Chem. Soc.* **1979**, *101*, 3842.
(5) Bino, A.; Cotton, F. A.; Dori, Z. *J. Am. Chem. Soc.* **1981**, *103*, 243.
(6) Bino, A.; Cotton, F. A.; Dori, Z.; Kolthammer, B. W. S. *J. Am. Chem. Soc.* **1981**, *103*, 5779.
(7) Bino, A.; Cotton, F. A.; Dori, Z.; Koch, S.; Küppers, H.; Millar, M.; Sekutowski, J. C. *Inorg. Chem.* **1978**, *17*, 3245.
(8) Murmann, R. K.; Shelton, M. E. *J. Am. Chem. Soc.* **1980**, *102*, 3984.
(9) Mattes, R.; Mennemann, K. *Z. Anorg. Allg. Chem.* **1977**, *437*, 175.
(10) Bino, A.; Hesse, K.-F.; Küppers, H. *Acta Crystallogr., Sect. B* **1980**, *B36*, 723.
(11) Chisholm, M. H.; Folting, K.; Huffman, J. C.; Kirkpatrick, C. C. *J. Am. Chem. Soc.* **1981**, *103*, 5967.
(12) Similar structural chemistry is already known with the element niobium. Cf.: Bino, A. *J. Am. Chem. Soc.* **1980**, *102*, 7990.
(13) Sheldrick, G. M. SHELX-77, University Chemical Laboratory, Cambridge, United Kingdom, 1977.
(14) Cromer, D. T.; Mann, J. B. *Acta Crystallogr., Sect. A* **1968**, *A24*, 321.
(15) Hall, M. B.; Fenske, R. F. *Inorg. Chem.* **1972**, *11*, 768.

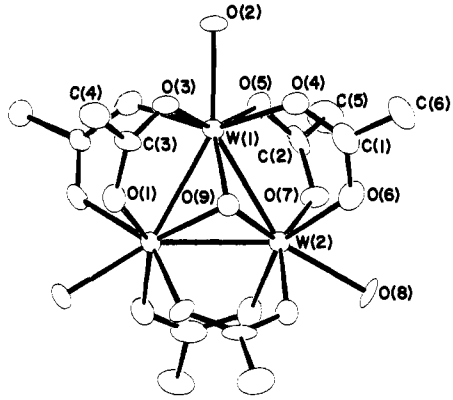

Figure 2. A perspective view of the trinuclear cation. For clarity, the disordered capping oxygen atom is shown only at one of its possible sites.

least-squares cycle. The atomic scattering factors for W and Zn were introduced as coefficients for analytical approximation of their scattering curves. The atomic scattering curves of Cromer and Mann[14] were used for C, O, and Br.

Molecular Orbital Calculations. These were carried out in a manner that has previously been described in detail[16,17] by use of the approximate Hartree–Foch method devised by Hall and Fenske.[15] As usual, W was replaced by Mo and CH_3 by H for practical reasons.

Spectral Measurements. The proton NMR spectrum was measured on a Varian A-60 spectrometer. The visible spectrum was recorded on a Varian Model 635 spectrophotometer using a solution of aqueous CF_3SO_3H. The following maxima were observed, with the wavelengths in nanometers and the decadic molar extinction coefficients, which are only approximate, given in parentheses: 340 (2375); 404 (1016); 508 (625); 668 (1250).

Results

Structure. The atomic positional parameters are listed in Table I, and the interatomic distances and angles obtained therefrom are listed in Tables II and III. The thermal parameters as well as the observed and calculated structure factors are available as supplementary material (see note at the end of this paper). The structure of the trinuclear cation and the atomic numbering scheme are shown in Figure 2.

There are four cations per unit cell. They lie with W(2) and O(8) on the crystallographic twofold axes that are parallel to the *b* axis and have crystallographic 2 (C_2) symmetry. This, of course, is inconsistent with the presence of only one capping oxygen atom per cluster unless these capping atoms are disordered. The solution and refinement of the structure proceeded in such a way as to show that this is the case.

A difference Fourier map based on all the non-hydrogen atoms except the capping group showed residual electron density of about 2.5 e $Å^{-3}$ above and below the W_3 triangle. When this density was refined as one-half oxygen, the temperature factor assumed a magnitude quite similar to those of all other oxygen atoms bonded to tungsten atoms.

Independent and very direct evidence that only one capping atom is present was obtained from the NMR spectrum. The ^1H NMR spectrum recorded at 60 mHz in D_2O solution shows that the cation is diamagnetic. It consists of two signals of equal intensites at 2.83 and 2.79 ppm downfield from tetramethylsilane. This clearly shows that the six acetate methyl groups are in two equally populated environments.

The measured density, 2.717 g cm^{-3}, is also closer to that calculated for the hemicapped cation, 2.711 g cm^{-3}, than to that calculated for a bicapped cation, 2.740 g cm^{-3}.

Discussion

Preparation. The hemicapped cluster cation is only a minor product under the reaction conditions we have used, with the major product being the bicapped cluster, $[W_3O_2(O_2CCH_3)_6(H_2O_3]^{2+}$.

Table III. Important Bond Angles (Degrees)

Br(1)-Zn-Br(2)	110.1 (1)		
W(1)'-W(1)-W(2)	60.17 (2)	W(1)-W(2)-O(6)	83.1 (3)
W(1)'-W(2)-W(1)	59.66 (3)	W(1)-W(2)-O(6)'	123.1 (3)
W(1)'-W(1)-O(11)	83.8 (3)	W(1)-W(2)-O(7)	83.6 (3)
W(1)'-W(1)-O(2)	150.5 (3)	W(1)-W(2)-O(7)'	123.6 (3)
W(1)'-W(1)-O(3)	82.9 (3)	W(1)-W(2)-O(8)	150.2 (1)
W(1)'-W(1)-O(4)	123.2 (3)	W(1)-W(2)-O(9)	45.3 (7)
W(1)'-W(1)-O(5)	122.6 (3)	W(1)-W(2)-O(9)'	46.1 (6)
W(1)'-W(1)-O(9)	46.5 (6)	O(6)-W(2)-O(6)'	151.6 (4)
W(1)'-W(1)-O(9)'	45.6 (7)	O(6)-W(2)-O(7)	88.8 (5)
W(2)-W(1)-O(1)'	123.9 (3)	O(6)-W(2)-O(7)'	84.0 (5)
W(2)-W(1)-O(2)	149.3 (3)	O(6)-W(2)-O(8)	75.8 (3)
W(2)-W(1)-O(3)	122.7 (3)	O(6)-W(2)-O(9)	127.4 (8)
W(2)-W(1)-O(4)	83.8 (3)	O(6)-W(2)-O(9)'	77.8 (8)
W(2)-W(1)-O(5)	82.6 (3)	O(7)-W(2)-O(7)'	150.5 (4)
W(2)-W(1)-O(9)	46.8 (6)	O(7)-W(2)-O(8)	75.3 (3)
W(2)-W(1)-O(9)'	46.7 (6)	O(7)-W(2)-O(9)	77.5 (7)
O(1)'-W(1)-O(2)	75.5 (5)	O(7)-W(2)-O(9)'	128.7 (7)
O(1)'-W(1)-O(3)	89.7 (4)	O(8)-W(2)-O(9)	143.6 (6)
O(1)'-W(1)-O(4)	150.2 (5)	W(1)-O(9)-W(1)'	87.9 (9)
O(1)'-W(1)-O(5)	83.3 (4)	W(1)-O(9)-W(2)	88 (1)
O(1)'-W(1)-O(9)	77.1 (7)	W(1)'-O(9)-W(2)	87.1 (8)
O(1)'-W(1)-O(9)'	128.3 (8)	W(1)'-O(1)-C(3)	125 (1)
O(2)-W(1)-O(3)	76.4 (4)	W(1)-O(3)-C(3)	126 (1)
O(2)-W(1)-O(4)	74.8 (4)	W(1)-O(4)-C(1)	125 (1)
O(2)-W(1)-O(5)	76.0 (4)	W(1)-O(5)-C(2)	128 (1)
O(2)-W(1)-O(9)	142.7 (7)	W(2)-O(6)-C(1)	125 (1)
O(2)-W(1)-O(9)'	143.0 (8)	W(2)-O(7)-C(2)	126 (1)
O(3)-W(1)-O(4)	82.3 (4)	O(4)-C(1)-O(6)	123 (2)
O(3)-W(1)-O(5)	152.4 (4)	O(4)-C(1)-C(6)	119 (2)
O(3)-W(1)-O(9)	128.3 (7)	O(6)-C(1)-C(6)	117 (1)
O(3)-W(1)-O(9)'	76.0 (7)	O(5)-C(2)-O(7)	120 (1)
O(4)-W(1)-O(5)	90.5 (4)	O(5)-C(2)-C(5)	122 (1)
O(4)-W(1)-O(9)	129.6 (7)	O(7)-C(2)-C(5)	118 (1)
O(4)-W(1)-O(9)'	77.5 (8)	O(1)-C(3)-O(3)	122 (1)
O(5)-W(1)-O(9)	76.1 (7)	O(1)-C(3)-C(4)	119 (1)
O(5)-W(1)-O(9)'	128.5 (7)	O(3)-C(3)-C(4)	119 (1)

Since there is as yet little understanding of those reactions between $Mo(CO)_6$ or $W(CO)_6$ with carboxylic acids that lead to the major products, it is hardly surprising that we do not yet know how to control, or improve, the yield of the $[W_3O(O_2CCH_3)_6(H_2O)_3]^{2+}$ ion. An understanding of the mechanism of these reactions will certainly be an objective in future work, but for the present we can more fruitfully turn to a discussion of the structure, properties, and bonding of the new trinuclear cation.

Structure. The structure of the $[W_3O(O_2CCH_3)_6(H_2O)_3]^{2+}$ ion is virtually identical with the previously reported structure of tritungsten clusters with two capping oxygen atoms except for the absence of one capping oxygen atom. Because of the crystallographic twofold axis passing through the W(2)–O(8) bond, the two chemically different sets of acetate groups are crystallographically equivalent. The entire $W_3(O_2CCH_3)_3(H_2O)_3$ portion of the cation shows no differences in bond lengths or bond angles on the capped side as compared to the uncapped side of the W_3 triangle. Although some small differences of this kind must surely exist, they are averaged out by the disorder in the position of the capping oxygen atom.

Of the quantitative differences between the hemicapped and the full bicapped structures, the largest and most unambiguous by far is in the W–W distances. In the four bicapped structures previously reported,[7,10] the W–W distances varied from 2.747 (1) to 2.769 (6) Å, with the grand average being 2.75 [1] Å.[18] In the present compound, the average distance is 2.710 [4] Å. This is clearly a significant difference in both the statistical and chemical senses. In fact, it constitutes additional significant evidence that the present compound is truly different from the known bicapped types.

The W–(μ_3-O) distances in this case range from 1.93 (2) to 1.98 (2) Å, averaging 1.96 [2] Å, while in the bicapped species

(16) Bursten, B. E.; Cotton, F. A.; Hall, M. B.; Najjar, R. C. *Inorg. Chem.* **1982**, *21*, 302.
(17) Cotton, F. A.; Fang, A. *J. Am. Chem. Soc.* **1982**, *104*, 113.

(18) We use (*x*) to indicate esd's and [*x*] to represent $[\sum\Delta_i^2/n(n-1)]^{1/2}$ where Δ_i is the difference of the *i*th individual value from the arithmetic mean of all values of a given bond length or angle making up a set of *n* such values.

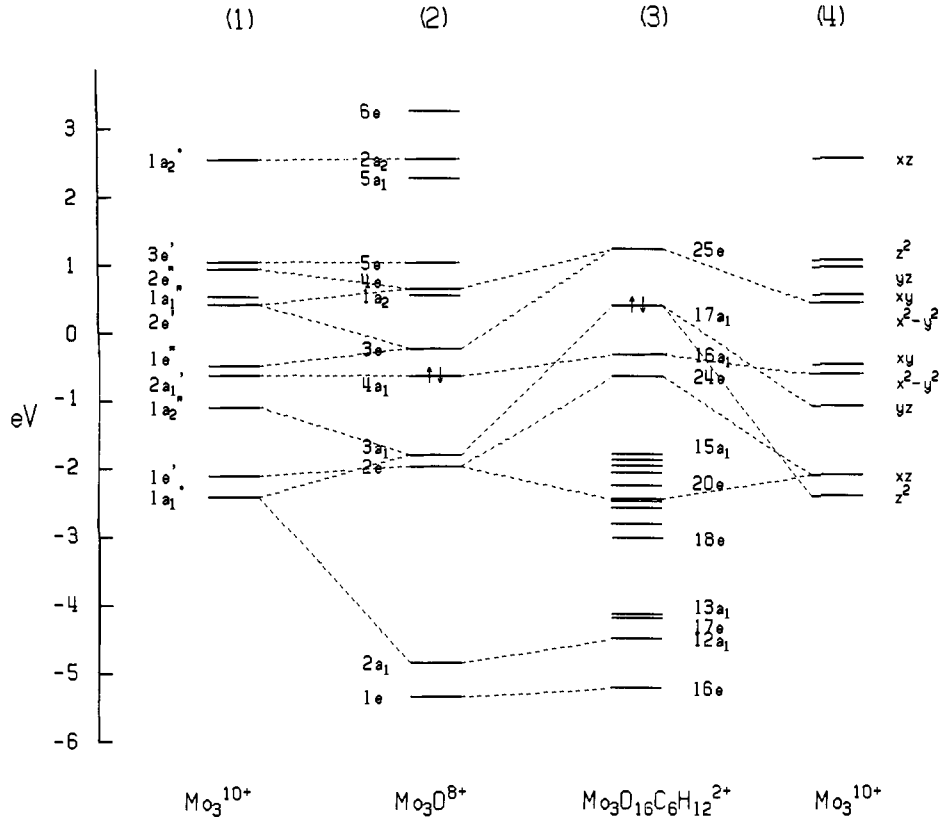

Figure 3. An energy-level diagram of the molecular orbitals for a bare Mo_3^{10+} cluster (columns 1 and 4), a Mo_3O^{8+} species (column 2), and an entire $[Mo_3O(O_2CH)_6(H_2O)_3]^{2+}$ ion (column 3).

the grand average value is 2.00 [1] Å. The apparent difference cannot be said to be significant. The W–O(acetate) distances here average 2.07 [1] Å, which is not significantly different from the average value of 2.09 [1] Å in the bicapped structures. For the W–O(water) distances, which average 2.16 [1] Å here, there is, apparently, a significant lengthening compared to the grand average value in the two $[W_3O_2(O_2CR)_6(H_2O)_3]^{2+}$ compounds of 2.11 [2] Å. This may result from the lower formal oxidation number, $3^1/_3$ in the present case vs. 4.0.

The tetrahedral $[ZnBr_4]^{2-}$ ion found in this structure has normal dimensions. It resides on a crystallographic twofold axis with a mean Zn–Br bond length of 2.41 [1] Å.

Electronic Structure. The Fenske–Hall molecular orbital calculations were performed to explore the consequences of removing one capping atom with respect to the bonding in the metal atom cluster. We know experimentally (from the NMR) that the resulting compound is diamagnetic and that the W–W distance, 2.710 [4] Å, is significantly shorter than in the bicapped structures, where they are 2.75 [1] Å. This does not necessarily imply that the W–W bonds are stronger, but it is consistent with such a possibility.

In proceeding from an $[M_3O_2(O_2CR)_6L_3]^{2+}$ to an $[M_3O(O_2CR)_6L_3]^{2+}$ species we are formally removing a neutral oxygen atom. Such a capping oxygen atom, whether unique or one of two, when it is in its place over the M_3 cluster is bound to the cluster in the following way. One electron pair occupies an MO (an a type) made up heavily of metal d orbitals and the oxygen p orbital, p_z, that points to the center of the metal triangle. This is a fairly covalent bond. Two more electron pairs occupy a doubly degenerate (e type) MO having some metal atom d character but predominantly oxygen atom p_x and p_y character. This is a more ionic bond. A qualitative way to describe the loss of the oxygen atom is to envision that it leaves with the two pair of electrons in the doubly degenerate orbital (plus its 2s electrons that are essentially localized on it to begin with), leaving behind the electron pair in the a-type MO. This pair of electrons would then have a more or less bonding effect with respect to the M_3 cluster. The now empty e-type orbital should be of intermediate energy with essentially nonbonding character.

While the foregoing qualitative picture, which has been developed intuitively by using the calculated results for the bicapped system[16] as a point of departure, is a reasonable one, we felt that a greater degree of detail was desirable. A quantitative calculation of the Fenske–Hall type was therefore carried out on the hemicapped system itself. The results are presented diagramatically in Figure 3. Tables of numerical results are available as Supplementary Material.

In columns 1 and 4 are plotted the energies of the metal cluster orbitals formed from the 15 metal d orbitals, and for each of these, the type of d orbital principally contributing to it is also indicated. In column 2 of Figure 3 are the MO's for the Mo_3O^{8+} unit, except for the $1a_1$ orbital, which is essentially the pure oxygen 2s atomic orbital. At about −5 eV we find the 1e and $2a_1$ orbitals, which account for the Mo_3–O bonding. In the case of an $Mo_3O_2^{8+}$ moiety,[16] there were four such orbitals (1e′, 1e″, $2a_1'$, and $2a_2''$) between −6 and −7 eV to account for the bonding of two O atoms to the Mo_3 cluster.

Next higher in energy, at about −2 eV, we find the 2e and $3a_1$ MO's, which are responsible for the set of Mo–Mo σ bonds. the former is made up 92% of the 1e′ orbital of the bare cluster, and the latter is derived 46% from the $1a_1'$ and 44% from the $1a_2''$ orbital of the bare cluster. These two orbitals, 2e and $3a_1$ of the Mo_3O^{8+} unit, are very comparable to the 2e′ and $3a_1'$ MO's that account for the Mo–Mo bonding in $Mo_3O_2^{8+}$. In $Mo_3O_2^{8+}$, the $3a_1'$ orbital is the HOMO.

In Mo_3O^{8+}, however, there is one more occupied MO, $4a_1$. This is derived almost entirely (95%) from the $2a_1'$ $(x^2 - y^2)$ MO of the bare cluster. Similarly, the LUMO in Mo_3O^{8+} is the 3e orbital. The former is weakly bonding, while the latter is essentially nonbonding. These two orbitals are the ones that would be used to form bonds to a second capping oxygen atom if one were present. Thus far, our qualitative picture of what should happen when the bicapped $Mo_3O_2^{8+}$ unit is converted to the hemicapped Mo_3O^{8+} unit is well supported by the calculation.

In Figure 4 are contour diagrams, drawn in the molecular plane, of the $3a_1$ and $4a_1$ MO's of Mo_3O^{8+}. The strongly Mo–Mo

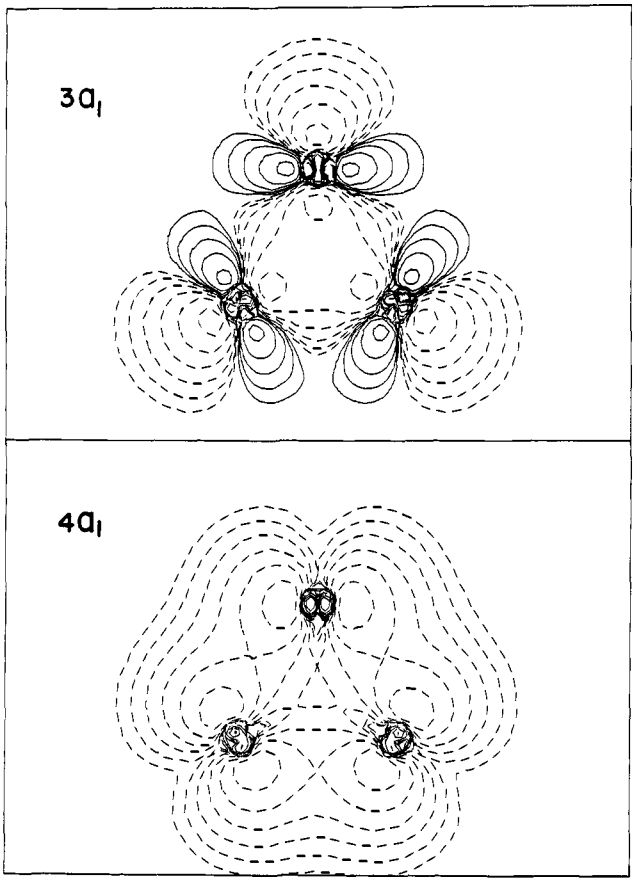

Figure 4. Contour maps, in the Mo_3 plane, of the $3a_1$ and $4a_1$ orbitals of the Mo_3O^{8+} ion. Contours begin at 0.0039 e Å^{-3} and increase by a factor of 2 at each step.

bonding character of the $3a_1$ orbital is evident, as is its parentage in atomic d_{z^2} and d_{yz} of the metal atoms. The $4a_1$ orbital is made up of atomic $d_{x^2-y^2}$ orbitals, and only the amplitude resulting from the lobes along the local x axes is revealed in the diagram. There are, of course, also lobes above and below the plane on each metal atom that are not seen here.

Let us turn now to the results for the complete $[Mo_3O(O_2CH)_6(H_2O)_3]^{2+}$ ion, which are presented in column 3 of Figure 3. As a result of the additional metal–ligand interactions, there are some changes in the ordering of the levels responsible for Mo–Mo bonding, but the bonding picture remains fundamentally the same as it was for Mo_3O^{8+}. In discussing the relationship between the MO's for the entire $[Mo_3O(O_2CH)_6(H_2O)_3]^{2+}$ ion and those of the Mo_3O^{8+} and Mo_3^{10+} moieties, we shall use bold symbols for the first and ordinary roman ones for the last two. The latter will be distinguishable from each other by virtue of the fact that for Mo_3^{10+}, with its D_{3h} symmetry, all symbols must carry either primes or double primes.

The HOMO of the $[Mo_3O(O_2CH)_6(H_2O)_3]^{2+}$ ion is the **17a**$_1$ orbital, which comes 57% from $3a_1$ and is otherwise built up from many other small contributions (each one ≤8%) from the other a_1 metal-based orbitals and from the ligands. If we trace the **17a**$_1$ orbital directly back to the Mo_2^{10+} unit, we find that it derives 40% from $1a_2''$ and 26% from $1a_1'$. A contour diagram of the **17a**$_1$ orbital would resemble that of the $3a_1$ orbital, shown in Figure 4. Thus, in summary, the HOMO of the full cation is principally a component of the Mo–Mo σ-bond system. Next below the **17a**$_1$ orbital is the **16a**$_1$ orbital, which is made up almost entirely (93%) of the $4a_1$ orbital, which, in turn, came 95% from the $2a_1'$ orbital. This **16a**$_1$ orbital thus contains what we have earlier described qualitatively as the pair of a-type electrons remaining when the O atom is removed from the bicapped structure. A contour diagrm of the **16a**$_1$ orbital would look essentially like that of the $4a_1$ orbital shown in Figure 4. The orbital has almost pure metal character.

The **24e** orbital is derived 51% from the 2e orbital plus contributions from various ligand orbitals. Further down is the **20e** orbital, which is derived 32% from the 2e orbital. Thus the e contribution to σ bonding in the Mo_3 cluster is supplied mainly by the **24e** orbital but also receives a significant contribution from the **20e** orbital. The other orbitals surrounding the **20e** orbital in the energy range −1.8 to −3.1 eV are HCO_2 orbitals.

The **12a**$_1$ and **16e** orbitals are closely related to the $2a_1$ and 1e orbitals and account for the Mo_3–μ_3-O bonding. Other orbitals below −4 eV in energy are Mo–O bonding orbitals and ligand orbitals.

The LUMO of the $[Mo_3O(O_2CH)_6(H_2O)_3]^{2+}$ ion is the **25e** orbital, which corresponds most closely to the 4e orbital of Mo_3O^{8+} (69%) although it derives partly (17%) from the 3e orbital. In terms of the Mo_3^{10+} orbitals, it arises mainly (67%) from 2e′ but also 14% from 2e″.

Color and Spectrum. The most obvious difference between the deep blue $[W_3O(O_2CCH_3)_6(H_2O)_3]^{2+}$ ion and the yellow to brown $[W_3O_2(O_2CR)_6L_3]$ species[7] is, of course, the colors. The spectrum explains this in terms of the strong absorption band in the red end of the visible region, 668 nm, with ϵ = 1250. We think it likely that the absorption band can be assigned to the **25e** ← **17a**$_1$ excitation. While this is an allowed $^1A_1 \rightarrow {}^1E$ transition, its intensity would be mitigated by the fact that it involves an electron jump between MO's derived largely from orthogonal d functions.

Summary. It has been found that a byproduct of the reaction of $W(CO)_6$ with a mixture of acetic acid and acetic anhydride containing a little triethylamine is a tritungsten cluster cation having only one capping oxygen atom but otherwise being essentially identical with the bicapped species, reported several years ago, which are the main reaction products. The new type of trinuclear cation, whose structure we have called the hemicapped type, has been isolated in the compounds $[W_3O(O_2CCH_3)_6(H_2O)_3]MBr_4 \cdot 8H_2O$ (M = Fe, Zn), and the crystal structure of the zinc salt has been determined. The W–W distance, 2.71 [1] Å, is significantly different from that, 2.75 [1] Å, in the bicapped cations. The NMR spectrum provides strong confirmation that only one capping oxygen is present. The electronic structure, bonding, and visible spectrum are well accounted for by a Fenske–Hall type molecular orbital calculation, which shows that in addition to six M–M bonding electrons comparable to those in the bicapped species, an additional electron pair occupies an a_1 orbital with weakly M–M bonding character.

Acknowledgment. We are grateful to the U.S.–Israeli Binational Science Foundation and the National Science Foundation for support. We thank Dr. W. Schwotzer for the NMR measurements and for checking the synthesis.

Registry No. $[W_3O(O_2CCH_3)_6(H_2O)_3]ZnBr_4 \cdot 8H_2O$, 82823-94-7; $[W_3O(O_2CCH_3)_6(H_2O)_3]FeBr_4$, 82823-95-8; $W(CO)_6$, 14040-11-0; $[Mo_3O(O_2CH)_6(H_2O)_3]^{2+}$, 82797-06-6; $[W_3O(O_2CCH_3)_6(H_2O)_3]^{2+}$, 82797-07-7.

Supplementary Material Available: A table of observed and calculated structure factors and a table of thermal vibration parameters (16 pages). Ordering information is given on any current masthead page.